PERGAMON

International Journal of Solids and Structures 39 (2002) 5123–5141

INTERNATIONAL JOURNAL OF SOLIDS and STRUCTURES

www.elsevier.com/locate/ijsolstr

A FE formulation for elasto-plastic materials with planar anisotropic yield functions and plastic spin

Chung-Souk Han [a,*], Yangwook Choi [b], June-K. Lee [b], R.H. Wagoner [a]

[a] *Department of Materials Science and Engineering, Ohio State University, 477 Watts Hall 2041, College Road, Columbus, OH 43210-1179, USA*

[b] *Department of Mechanical Engineering, Ohio State University, 206 West 18th Avenue, Columbus, OH 43210-1179, USA*

Received 8 January 2002; received in revised form 2 July 2002

Abstract

In this article a stress integration algorithm for shell problems with planar anisotropic yield functions is derived. The evolution of the anisotropy directions is determined on the basis of the plastic and material spin. It is assumed that the strains inducing the anisotropy of the pre-existing preferred orientation are much larger than subsequent strains due to further deformations. The change of the locally preferred orientations to each other during further deformations is considered to be neglectable. Sheet forming processes are typical applications for such material assumptions. Thus the shape of the yield function remains unchanged. The size of the yield locus and its orientation is described with isotropic hardening and plastic and material spin.

The numerical treatment is derived from the multiplicative decomposition of the deformation gradient and thermodynamic considerations in the intermediate configuration. A common formulation of the plastic spin completes the governing equations in the intermediate configuration. These equations are then pushed forward into the current configuration and the elastic deformation is restricted to small strains to obtain a simple set of constitutive equations. Based on these equations the algorithmic treatment is derived for planar anisotropic shell formulations incorporating large rotations and finite strains. The numerical approach is completed by generalizing the Return Mapping algorithm to problems with plastic spin applying Hill's anisotropic yield function. Results of numerical simulations are presented to assess the proposed approach and the significance of the plastic spin in the deformation process.

Keywords: Anisotropic material; Elastic–plastic material; Finite strain; Shells

1. Introduction

In the plasticity related literature some articles consider whether or not the plastic spin has to be applied for a correct formulation of stress rates (see e.g., Haupt and Tsakmakis, 1986; Simo, 1988; Lubarda and Shih, 1994; Dafalias, 1998; Van der Giessen, 1991). Following the investigations in Haupt and

* Corresponding author. Fax: +1-1614-292-6530.
E-mail address: han.136@osu.edu (C.-S. Han).

0020-7683/02/$ - see front matter
PII: S0020-7683(02)00421-3

Tsakmakis (1986), the plastic spin in this presentation is not applied for the description of the stress rates; the convective (Oldroyd, 1950) rate is used instead. The plastic spin is, however, applied to describe the evolution of the directions of the anisotropic yield function.

Such reorientations of the anisotropy axes can be easily motivated by observing the plastic deformation of single crystals, where the active slip planes rotate with the plastic deformation, while the material spin may be zero (see e.g., Asaro, 1983). The reorientation of anisotropy axes of a polycrystal can be understood as the mean rotation of the single crystals in a polycrystal aggregate. From experimental results in the literature it could be concluded that the plastic spin can be neglectable for polycrystalline aluminum since maximal rotations of up to 5° at 20% strain have been reported in Bunge and Nielsen (1997) and Truong Qui and Lippmann (2001). For mild steel this seems not be valid—maximal rotations of up to 45° at 10% strains were observed in Boehler and Koss (1991) and Kim and Yin (1997).

Although the reorientation of anisotropic directions seems apparent for steel sheet metals, proper computational treatments for practical applications particularly in sheet forming processes are quite rare. Different approaches to describe the anisotropy direction can be found in the literature. Loret (1983), Lee et al. (1995), Steinmann et al. (1996) and Dafalias (1998) used structural tensors to define the anisotropy directions. A different description has been applied in Yoon et al. (1999) and Tugcu and Neale (1999), where motivated from rigid-plastic formulations (see Yang and Kim, 1986; Chung and Shah, 1992), the orientation of the yield function remains directly expressed by its directional material axes. These formulations can also be derived in a multiplicative setting as exposed in Han et al. (in press). Based on this formulation an algorithmic treatment for shell problems incorporating kinematic hardening has been presented in Han et al. (submitted).

In this paper an algorithmic treatment for FE-shell formulations incorporating the plastic spin is presented. It is assumed that the strains inducing the anisotropy of the pre-existing preferred orientation are much larger than subsequent strains because of further deformations. The change of the locally preferred orientations to each other as a result of further deformations is considered to be neglectable (see Hill, 1950). Sheet forming processes are typical applications for such material assumptions. The derivation of the algorithmic treatment is achieved on the basis of the multiplicative decomposition of the deformation gradient and thermodynamic considerations in the intermediate configuration. A common formulation of the plastic spin, first suggested in Zbib and Aifantis (1988), completes the governing equations in the intermediate configuration. These equations are then pushed forward into the current configuration and the elastic deformation is restricted to small strains to obtain a simple set of constitutive equations. Based on these equations the algorithmic treatment is derived for planar anisotropic shell formulations incorporating large rotations and finite strains. To this aim the Return Mapping algorithm is generalized for material models with plastic spin and Hill's (1950) anisotropic yield function. The results of numerical examples are presented and discussed to assess the proposed approach.

2. Material formulation

2.1. Clausius–Duhem inequality

The generalization of the additive decomposition in the small strain case to finite strains is commonly motivated by the structure of the single crystal model for metal plasticity (Lee, 1969), and shall be stated here as $\mathbf{F} = \mathbf{F}_e\mathbf{F}_p$. The resulting kinematic relations and stress and strain expressions related to the intermediate configuration $\overline{\mathscr{B}}$ are listed in Table 1. These expressions will be used to formulate the Clausius–Duhem inequality in the following.

The stress power $\mathscr{W}$ per unit reference volume is described by $\mathscr{W} = \mathbf{S} \cdot \dot{\mathbf{E}} = \boldsymbol{\tau} \cdot \mathbf{d}$, with the second Piola–Kirchhoff tensor $\mathbf{S}$, the Green–Lagrangian tensor $\mathbf{E} = (1/2)(\mathbf{F}^T\mathbf{F} - \mathbf{1})$ defined in $\mathscr{B}_o$ and their counterparts

Table 1
Kinematic relations and stress/strain-expressions in $\overline{\mathscr{B}}$

Multiplicative decomposition	$\mathbf{F} = \mathbf{F}_e\mathbf{F}_p$	(46)
Velocity gradient	$\mathbf{l} = \mathbf{l}_e + \mathbf{F}_e\overline{\mathbf{L}}_p\mathbf{F}_e^{-1}$	(47)
	with $\mathbf{l}_e = \dot{\mathbf{F}}_e\mathbf{F}_e^{-1}$ and $\overline{\mathbf{L}}_p = \dot{\mathbf{F}}_p\mathbf{F}_p^{-1}$	(48)
Plastic velocity gradient	$\overline{\mathbf{L}}_p = \overline{\mathbf{D}}_p + \overline{\mathbf{W}}_p$	(49)
	with $\overline{\mathbf{D}}_p = (\overline{\mathbf{L}}_p)_S$ and $\overline{\mathbf{W}}_p = (\overline{\mathbf{L}}_p)_A$	(50)
Lagrangian strain tensor	$\overline{\mathbf{E}} = \frac{1}{2}(\mathbf{F}_e^T\mathbf{F}_e - \mathbf{F}_p^{-T}\mathbf{F}_p^{-1}) = \overline{\mathbf{E}}_e + \overline{\mathbf{E}}_p$	(51)
	with $\overline{\mathbf{E}}_e = \frac{1}{2}(\mathbf{F}_e^T\mathbf{F}_e - \mathbf{1})$	(52)
	and $\overline{\mathbf{E}}_p = \frac{1}{2}(\mathbf{1} - \mathbf{F}_p^{-T}\mathbf{F}_p^{-1})$	(53)
Second Piola–Kirchhoff stress	$\overline{\mathbf{S}} = \mathbf{F}_e^{-1}\boldsymbol{\tau}\mathbf{F}_e^{-T}$	(54)
Mandel stress	$\overline{\mathbf{P}} = (\mathbf{1} + 2\overline{\mathbf{E}}_e)\overline{\mathbf{S}} = \overline{\mathbf{C}}_e\overline{\mathbf{S}}$	(55)
Oldroyd rate for strain like tensors	$(.)^{\bar{\Delta}} = (.) + \overline{\mathbf{L}}_p^T(.)^{\cdot} + (.)\overline{\mathbf{L}}_p$	(56)
Oldroyd rate for stress like tensors	$(.)^{\bar{\nabla}} = (.) - \overline{\mathbf{L}}_p(.)^{\cdot} - (.)\overline{\mathbf{L}}_p^T$	(57)

in $\mathscr{B}$ as the rate of deformation tensor $\mathbf{d} = (1/2)(\mathbf{l} + \mathbf{l}^T)$ and the Kirchhoff stress tensor $\boldsymbol{\tau} = \det(\mathbf{F})\boldsymbol{\sigma}$. The stress power in the intermediate configuration $\overline{\mathscr{B}}$ can be reformulated as

$$\mathscr{W} = \overline{\mathbf{S}} \cdot \overline{\mathbf{E}}^{\bar{\Delta}}, \tag{1}$$

with $\overline{\mathbf{S}}$ defined by (54) and the Oldroyd derivative (56) of $\overline{\mathbf{E}}$ defined by (51) (see Haupt and Tsakmakis, 1986). The Clausius–Duhem inequality for isothermal processes can be stated as $\mathscr{W} - \dot{\psi} \geqslant 0$ with the specific free energy function ψ. This inequality can be expressed by

$$\overline{\mathbf{S}} \cdot \overline{\mathbf{E}}^{\bar{\Delta}} - \dot{\psi} \geqslant 0 \tag{2}$$

in the intermediate configuration.

An additive split of the free energy function is assumed $\psi(t) = \psi_e(t) + \psi_p(t)$, with the elastic part ψ_e to be isotropic and dependent on $\mathbf{F}_e$. The time derivative of ψ_e is given with $\dot{\psi}_e = (\partial\bar{\psi}_e/\partial\overline{\mathbf{E}}_e) \cdot \dot{\overline{\mathbf{E}}}_e$, which yields, with $\overline{\mathbf{S}} = \partial\bar{\psi}_e/\partial\overline{\mathbf{E}}_e$ and the plastic part of the Oldroyd derivative of the Green–Lagrangian strain tensor $\overline{\mathbf{D}}_p = \overline{\mathbf{E}}_p^{\Delta}$ to the reduced form of (2),

$$\mathscr{D} = \overline{\mathbf{P}} \cdot \overline{\mathbf{D}}_p - \dot{\psi}_p \geqslant 0, \tag{3}$$

where $\mathscr{D}$ denotes the local internal dissipation function (see Han et al., submitted for details).

2.2. Evolution of plastic rate of deformation and hardening

Anisotropic yield functions shall be incorporated in the proposed material model. Within this approach their orientation will be described with directional axes $\bar{\mathbf{e}}_i^{\phi}$, $i = 1, 2, 3$ in $\overline{\mathscr{B}}$ (see Fig. 1) which may evolve in the deformation process. We assume that the strains inducing the pre-existing preferred orientation are much larger than subsequent strains due to further deformations. Sheet forming processes are typical applications for such material assumptions. The change of the locally preferred orientations to each other during further deformations in such processes is considered to be neglectable (see Hill, 1950 or Kim and

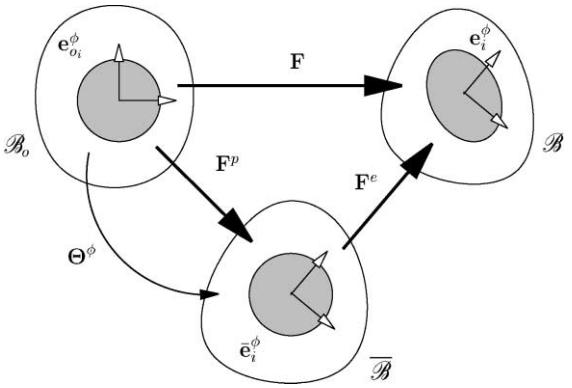

Fig. 1. Rotation of the directional axes of the anisotropic yield function.

Yin, 1997). The evolution of these orientations of the anisotropic yield function is related to the spin $\mathbf{\Theta}^{\phi}$ to be described in Section 2.3.

The isotropic plastic part of ψ_{p} is assumed to be dependent on a strain-like variable α. The thermo-conjugated variable to α is commonly defined with $q = -\partial\psi_{\mathrm{p}}/\partial\alpha$, which is of scalar stress type and describes the current yield strength. The time derivative of the isotropic part of the plastic free energy function is then simply stated by $\dot{\psi}_{\mathrm{p}} = -q\dot{\alpha}$. The evolution equations are derived on the basis of the local internal dissipation function (3) which can be written as

$$\mathscr{D} = \overline{\mathbf{P}} \cdot \overline{\mathbf{D}}_{\mathrm{p}} + q\dot{\alpha} \geqslant 0. \tag{4}$$

The yield locus Φ is considered to be convex and to be defined in $\overline{\mathscr{B}}$. If the yield function is anisotropic the orientation of the yield function is presumed to be defined by the axes of anisotropy $\bar{\mathbf{e}}^{\phi}_{i}$. This yield function is defined to have the deviatoric part of the Mandel stress tensor $\overline{\mathbf{P}}$ and the internal stress like variable q as its arguments

$$\Phi = \Phi(\overline{\mathbf{P}}^{D}, q; \bar{\mathbf{e}}^{\phi}_{i}) = \bar{\phi}(\overline{\mathbf{P}}^{D}; \bar{\mathbf{e}}^{\phi}_{i}) + q = 0. \tag{5}$$

Applying the postulate of maximal dissipation, the model of associative plasticity is obtained by solving

$$(\overline{\mathbf{P}} - \overline{\mathbf{P}}^{\star}) \cdot \overline{\mathbf{D}}_{\mathrm{p}} + (q - q^{\star})\dot{\alpha} \geqslant 0 \tag{6}$$

for all $(\overline{\mathbf{P}}^{\star}, q^{\star}) \in \mathbb{E} = \{(\overline{\mathbf{P}}, q) | \bar{\phi}(\overline{\mathbf{P}}; \bar{\mathbf{e}}^{\phi}_{i}) + q \leqslant 0\}$. This yields the evolution equations

$$\overline{\mathbf{D}}_{\mathrm{p}} = \dot{\gamma}\frac{\partial\bar{\phi}}{\partial\overline{\mathbf{P}}}, \tag{7}$$

$$\dot{\alpha} = \dot{\gamma} \tag{8}$$

and the Kuhn Tucker conditions $\dot{\gamma} \geqslant 0$, $\Phi \leqslant 0$, $\dot{\gamma}\Phi = 0$ for the solution of this restricted optimization problem. The consistency parameter $\dot{\gamma}$ can be viewed in the context of a restricted optimization problem, stated with (6), as a Lagrange multiplier. To ensure the symmetry of $\overline{\mathbf{D}}_{\mathrm{p}}$ the derivation of the yield function $\bar{\phi}$ with respect to $\overline{\mathbf{P}}$ has to be symmetric, which is assumed here. This holds for commonly used orthotropic yield functions as formulated by Hill (1950) if the yield function is written in terms of the Mandel stress tensor instead of the original Cauchy stress tensor.

By introducing the increment of the plastic arc length $\dot{s}$ the consistency parameter can also be described as $\dot{\gamma} = \dot{s}/\beta$ with $\dot{s} = \sqrt{\frac{2}{3}}\|\overline{\mathbf{D}}_{\mathrm{p}}\|$ and $\beta = \sqrt{\frac{2}{3}}\left\|\frac{\partial \bar{\phi}}{\partial \overline{\mathbf{P}}}\right\|$.

2.3. Evolution of the directional axes

The definition of the intermediate stress-free configuration $\overline{\mathscr{B}}$ is not unique because a rigid body rotation of this configuration results in the same deformation gradient. To define its orientation an interpretation of the multiplicative decomposition in the context of crystal plasticity is given, e.g., in Asaro (1983). Here we choose without loss of generality the elastic part of the deformation gradient to be symmetric, as applied also in Lee (1969) or Boyce et al. (1989). With this decomposition the plastic part of the deformation gradient $\mathbf{F}_{\mathrm{p}} = \widetilde{\mathbf{R}}_{\mathrm{e}}\widetilde{\mathbf{F}}_{\mathrm{p}} = \mathbf{R}_{\star}\mathbf{U}_{\mathrm{p}}$ describes the plastic shearing as well as the lattice rotation (see Fig. 2). Thus we arrive at

$$\mathbf{F} = \mathbf{F}_{\mathrm{e}}\mathbf{F}_{\mathrm{p}} = \mathbf{V}_{\mathrm{e}}\mathbf{R}_{\star}\mathbf{U}_{\mathrm{p}}. \tag{9}$$

Generally arbitrary approaches can be applied for the development of the anisotropy axes without violating the thermodynamic restriction (3). Although $\overline{\mathbf{W}}_{\mathrm{p}}$ does not enter the local dissipation function $\mathscr{D}$, it is known that for crystals the plastic strain rate $\overline{\mathbf{D}}_{\mathrm{p}}$ and the spin in single slip are directly coupled. In general, the spin should be considered dependent on the parameters describing plastic flow and on material properties like the mean orientation of the grains of a polycrystal. To formulate such a dependency the antisymmetric part of the plastic velocity gradient $(\overline{\mathbf{L}}_{\mathrm{p}})_{\mathbf{A}} = \overline{\mathbf{W}}_{\mathrm{p}}$ relative to $\overline{\mathscr{B}}$ is decomposed as

$$\overline{\mathbf{W}}_{\mathrm{p}} = \overline{\mathbf{\Theta}}^{\phi}_{\mathrm{p}} + \overline{\mathbf{\Omega}}^{\phi}_{\mathrm{p}}, \tag{10}$$

where, referring to Dafalias (2000), $\overline{\mathbf{W}}_{\mathrm{p}}$ is denoted as material spin, $\overline{\mathbf{\Theta}}^{\phi}_{\mathrm{p}}$ as constitutive spin, and $\overline{\mathbf{\Omega}}^{\phi}_{\mathrm{p}}$ as plastic spin. The description of the rotation of the directional axes $\mathbf{R}_{\phi}$ is related to $\overline{\mathbf{\Theta}}^{\phi}_{\mathrm{p}} = \dot{\mathbf{R}}_{\phi}\mathbf{R}^{\mathrm{T}}_{\phi}$ which is implicitly defined by the objective plastic spin tensor $\overline{\mathbf{\Omega}}^{\phi}_{\mathrm{p}}$.

Heuristic descriptions for $\overline{\mathbf{\Omega}}^{\phi}_{\mathrm{p}}$ have been proposed by several authors (e.g., Dafalias, 1985; Van der Giessen, 1991; Kuroda, 1997). A common description of the plastic spin would correspond to

$$\overline{\mathbf{\Omega}}^{\phi}_{\mathrm{p}} = \mu^{\phi}(\overline{\mathbf{P}}\overline{\mathbf{D}}_{\mathrm{p}} - \overline{\mathbf{D}}_{\mathrm{p}}\overline{\mathbf{P}}) \tag{11}$$

in the intermediate configuration, where the variable μ^{ϕ} can be a nonlinear function in $\overline{\mathbf{P}}$, $\overline{\mathbf{D}}_{\mathrm{p}}$ and $\bar{\mathbf{e}}^{\phi}_{i}$ and may also change its sign within the deformation process. For rigid plastic materials (11) was derived in

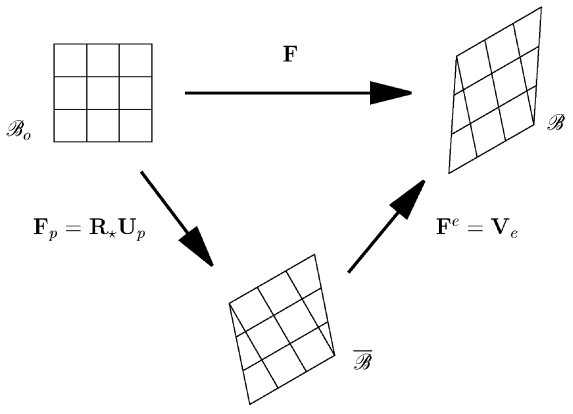

Fig. 2. Multiplicative decomposition by $\mathbf{F} = \mathbf{F}_{\mathrm{e}}\mathbf{F}_{\mathrm{p}} = \mathbf{V}_{\mathrm{e}}\mathbf{R}_{\star}\mathbf{U}_{\mathrm{p}}$.

Table 2
Evolution and spin equations in $\overline{\mathscr{B}}$

Evolution equations	$\overline{\mathbf{D}}_{\mathrm{p}} = \dot{\gamma}\dfrac{\partial\bar{\phi}}{\partial\overline{\mathbf{P}}}$
	$\dot{\alpha} = \dot{\gamma}$
Plastic spin	$\overline{\boldsymbol{\Omega}}_{\mathrm{p}}^{\phi} = \mu^{\phi}\overline{\mathbf{P}}\,\overline{\mathbf{D}}_{\mathrm{p}} - \overline{\mathbf{D}}_{\mathrm{p}}\overline{\mathbf{P}})$

Levitas (1998) on the basis of stability considerations. Physically this means that the plastic spin is present as long as $\overline{\mathbf{P}}$ and $\overline{\mathbf{D}}_{\mathrm{p}}$ are not colinear. In the context of the maximal plastic dissipation, the plastic spin will rotate the anisotropy axes into a more favorable energetic direction.

For μ^{ϕ} in (11) a simple approach has been suggested by Kuroda (1997)

$$\mu^{\phi} = c_K/\bar{\phi}, \tag{12}$$

with a material constant c_K and $\bar{\phi}$ representing the yield stress. A comparison of such an approach with experimental results, exposed in Kim and Yin (1997), has been discussed in Dafalias (2000) and yielded qualitatively good predictions of the rotation angles. The determination of the rotations of the anisotropy axes of the considered pre-stretched mild steel is performed by parameter fitting with respect to Hill's yield function (1950) yielding rotations of up to 45° in Kim and Yin (1997) at 10% strain. Similar results were obtained earlier in Boehler and Koss (1991) where it was also observed that the symmetry axes of the crystallographic texture rotate in about the same magnitude as in macroscopic tests of the steel sheets. Micromechanical investigations of aluminum sheets have been described in Bunge and Nielsen (1997) where the spin is understood as an averaged rotation of the symmetry axes caused by the rotating single crystals in the plastic deformation. The rotations of the symmetry axes are determined by texture description via Oriental Distribution Functions (see Bunge, 1982). Maximal rotations of only up to 5° at 20% strain were observed with this procedure. These values were also obtained by Truong Qui and Lippmann (2001) using macroscopic testing. Thus, for aluminum polycrystals the plastic spin appears to be of minor importance. From experiments (Boehler and Koss, 1991; Kim and Yin, 1997; Truong Qui and Lippmann, 2000) this is, however, not valid for steel. For steel sheets the plastic spin should be incorporated into the material description.

With the description of the plastic spin the formulation referred to the intermediate configuration $\overline{\mathscr{B}}$ is complete. The governing equations have been summarized in Table 2.

2.4. Transformation to the current configuration $\mathscr{B}$

The evolution equations formulated in the previous subsection describe all needed rates to describe the material formulation. However, one could consider a formulation in the nonphysical intermediate configuration disadvantageous because the yield function is defined in the stress free configuration $\overline{\mathscr{B}}$. Common yield functions, as in Barlat et al. (1991) and Hill (1950), are also all naturally defined in the current configuration $\mathscr{B}$. For an outline of the results obtained so far the transformation into $\mathscr{B}$ will be given in the following.

The Kirchhoff stress tensor $\boldsymbol{\tau}$ can be derived from $\overline{\mathbf{S}} = \mathbf{V}_{\mathrm{e}}^{-1}\boldsymbol{\tau}\mathbf{V}_{\mathrm{e}}^{-1}$ and (55), and yields $\boldsymbol{\tau} = \mathbf{V}_{\mathrm{e}}^{-1}\overline{\mathbf{P}}\mathbf{V}_{\mathrm{e}}$, which is symmetric because $\mathbf{V}_{\mathrm{e}}$ is coaxial to $\overline{\mathbf{P}}$ for elastic isotropy and yields $\boldsymbol{\tau} = \overline{\mathbf{P}}$. A corresponding push forward transformation of $\overline{\mathbf{D}}_{\mathrm{p}}$ (7) into the current configuration yields

$$\hat{\mathbf{d}}_{\mathrm{p}} = \frac{\dot{s}}{\beta}\mathbf{V}_{\mathrm{e}}^{-1}\frac{\partial\bar{\phi}}{\partial\overline{\mathbf{P}}}\mathbf{V}_{\mathrm{e}}^{-1}. \tag{13}$$

Although $\boldsymbol{\tau}$ and $\overline{\mathbf{P}}$ are identical for the considered case of isotropic elasticity the yield functions are not identical in the intermediate $\bar{\phi}$ and in the current configuration ϕ. The yield function is defined with the axes of anisotropy transferred to $\mathscr{B}$ which change with $\mathbf{V}_e$. It has to be observed that the axes of anisotropy $\mathbf{g}_i^{\phi}$ in $\mathscr{B}$ are no longer orthonormal since they transform via $\mathbf{g}_i^{\phi} = \mathbf{V}_e\bar{\mathbf{e}}_i^{\phi}$ and now obey $\mathbf{b}_e^{-1}$ as metric. Hence, the spin defining the evolution of $\mathbf{g}_i^{\phi}$ has to be described with $\mathbf{V}_e$ and its rate.

With these considerations an evaluation of the stresses in terms of the intermediate configuration $\overline{\mathscr{B}}$ in the previous subsection will be easier to deal with and more advantageous because all relevant physical terms can easily be pushed forward with $\mathbf{V}_e$ to $\mathscr{B}$. Recalling, however, that in most problems in metal plasticity the elastic strains can be considered to be small, the difficulties involved with such a formulation in $\mathscr{B}$ can be circumvented by confining the regarded problems to these cases.

Remark. We should emphasize here that $\hat{\mathbf{d}}_p$ in (13) should generally not be identified with the plastic rate of deformation referred to $\mathscr{B}$, defined by $\mathbf{d}_p = (\mathbf{l}_p)_S$, which can be easily seen by $\hat{\mathbf{d}}_p = \mathbf{V}_e^{-1}\overline{\mathbf{D}}_p\mathbf{V}_e^{-1} \neq (\mathbf{V}_e\overline{\mathbf{L}}_p\mathbf{V}_e^{-1})_S = (\mathbf{l} - \mathbf{l}_e)_S = (\mathbf{l}_p)_S = \mathbf{d}_p$. With the Almansi strain tensor $\mathbf{e} = (1/2)(\mathbf{1} - \mathbf{F}^{-T}\mathbf{F}^{-1})$ the push forward transformation in (13) can be viewed as the Oldroyd derivative of its elastic $\mathbf{e}_e = (1/2)(\mathbf{1} - \mathbf{V}_e^{-1}\mathbf{V}_e^{-1})$ and plastic strains $\mathbf{e}_p = (1/2)(\mathbf{V}_e^{-1}\mathbf{V}_e^{-1} - \mathbf{F}^{-T}\mathbf{F}^{-1})$ (see Haupt and Tsakmakis, 1986). Eq. (13) then simply states the push forward transformation $\hat{\mathbf{d}}_p = \mathbf{e}_p^{\Delta} = \mathbf{V}_e^{-1}\overline{\mathbf{D}}_p\mathbf{V}_e^{-1}$ from the intermediate to the current configuration, since $\overline{\mathbf{E}}_p^{\Delta} = \overline{\mathbf{D}}_p$. The Oldroyd derivative relative to $\mathscr{B}$ for $\mathbf{e}_p$ is thereby defined by $(.)^{\Delta} = (.) + \mathbf{l}^T(.) + (.)\mathbf{l}$.

Small elastic strains. In the following we restrict ourselves to small elastic strains, i.e. $\mathbf{F}_e = \mathbf{V}_e \approx \mathbf{1} + \mathscr{O}(\boldsymbol{\varepsilon}_e)$, framing a good approximation for a large range of problems in metal plasticity. This restriction yields the different plastic deformation rates to be approximately identical $\hat{\mathbf{d}}_p = \overline{\mathbf{D}}_p = \mathbf{d}_p$; and likewise the stress relations for small elastic strains can be stated by $\boldsymbol{\tau} = \overline{\mathbf{S}} = \overline{\mathbf{P}}$. For the directional axes we obtain

$$\mathbf{e}_i^{\phi} = \bar{\mathbf{e}}_i^{\phi}, \tag{14}$$

remaining perpendicular to each other because $\mathbf{R}_* \approx \mathbf{R} = \mathbf{F}\mathbf{U}^{-1}$. With the Kirchhoff stress tensor now directly related to the Mandel stress tensor and (14) the flow rule (7) can be written as

$$\mathbf{d}_p = \dot{\gamma}\frac{\partial\phi}{\partial\boldsymbol{\tau}}, \tag{15}$$

where we can identify $\dot{\gamma}$ as $\dot{\gamma} = \dot{s}/\beta$ with $\beta = \sqrt{\frac{2}{3}}\left\|\frac{\partial\phi}{\partial\boldsymbol{\tau}}\right\|$ and $\dot{s} = \sqrt{\frac{2}{3}}\|\mathbf{d}_p\|$. With the definitions of the elastic and plastic strains (51) in $\overline{\mathscr{B}}$ and the Oldroyd rate, (15) motivates the additive relation $\mathbf{d}_e = \mathbf{d} - \mathbf{d}_p$. The relations for the isotropic hardening (8) remain obviously unchanged.

The plastic and constitutive spin relative to the current configuration $\mathscr{B}$ simplifies to

$$\boldsymbol{\omega}_p^{\phi} = \overline{\boldsymbol{\Omega}}_p^{\phi} \quad \text{and} \quad \boldsymbol{\theta}^{\phi} = \overline{\boldsymbol{\Theta}}_p^{\phi}, \tag{16}$$

which consequently results in $\mathbf{w} = \overline{\mathbf{W}}_p$ and $\mathbf{w} = \boldsymbol{\theta}^{\phi} + \boldsymbol{\omega}_p^{\phi}$ for the material spin. Therefore, in the case of small elastic strain, the total spin is identical to the material spin of the intermediate configuration.

The governing equations relative to $\mathscr{B}$ confined to small elastic strain are summarized in Table 3.

Table 3
Evolution and spin equations in $\mathscr{B}$ for small elastic strains

Evolution equations	$\mathbf{d}_p = \dot{\gamma}\frac{\partial\phi}{\partial\boldsymbol{\tau}}$
	$\dot{\alpha} = \dot{\gamma}$
Plastic spin	$\boldsymbol{\omega}_p^{\phi} = \mu^{\phi}(\boldsymbol{\tau}\mathbf{d}_p - \mathbf{d}_p\boldsymbol{\tau})$

3. Shell kinematics

A finite element formulation of the shell continuum is considered to be applicable to structural problems with finite rotations and large strains. An arbitrary point in the deformed shell space is determined by $\mathbf{x}(\xi^1, \xi^2, \zeta) = \boldsymbol{\varphi}(\xi^1, \xi^2) + \zeta \mathbf{t}(\xi^1, \xi^2)$, where $\boldsymbol{\varphi}$ denotes the shell mid-surface and $\mathbf{t}$ is an inextensible director of unit length. The curvilinear base vectors tangent to ξ^1, ξ^2, ζ are given by

$$\mathbf{g}_\alpha = \boldsymbol{\varphi}_{,\alpha} + \zeta \mathbf{t}_{,\alpha}, \quad \text{and} \quad \mathbf{g}_3 = \mathbf{t}, \tag{17}$$

where $\alpha = 1, 2$. A strain measure, with respect to the reference configuration, is provided by the right Cauchy–Green tensor $\mathbf{C}$, with $C_{ij} = \mathbf{g}_i \cdot \mathbf{g}_j$, $i, j = 1, 2, 3$ being the covariant components of $\mathbf{C}$. The right Cauchy–Green tensor $\mathbf{C}$ can be split into membrane (m), shear (s) and bending (b) parts, yielding $\mathbf{C} = \mathbf{C}^{\mathrm{m}} + \mathbf{C}^{\mathrm{s}} + \zeta \mathbf{C}^{\mathrm{b}}$. The quadratic terms in ζ are neglected due to the thin shell limit. The relevant components of the different parts of $\mathbf{C}$ can be written as

$$C^m_{\alpha\beta} = \boldsymbol{\varphi}_{,\alpha} \cdot \boldsymbol{\varphi}_{,\beta}, \quad C^s_{\alpha 3} = 2\, \boldsymbol{\varphi}_{,\alpha} \cdot \mathbf{t}, \quad \text{and} \quad C^b_{\alpha\beta} = \boldsymbol{\varphi}_{,\alpha} \cdot \mathbf{t}_{,\beta} + \boldsymbol{\varphi}_{,\beta} \cdot \mathbf{t}_{,\alpha}. \tag{18}$$

Several parameterizations of the director $\mathbf{t}$ can be found in the literature. An inextensible director formulations is applied here, incorporating the classical assumption $S_{33} = 0$. Such formulations frame a good approximation widely applied for nonlinear shell problems (e.g., Wagner and Gruttmann, 1994; Hauptmann and Schweizerhof, 1998). With the additional condition that the shear strain $E_{\alpha 3}$ is small, we arrive at the Kirchhoff shell theory. This model can be approximately achieved with a penalty constraint for $E_{\alpha 3}$, as has been done in Eberlein and Wriggers (1999) and Han and Wriggers (2000), or by assuming a linear relation $S_{\alpha 3} = GE_{\alpha 3}$ with the shear modulus G used in other descriptions. Thus all relevant components for a material description of (18) are contained in $C^m_{\alpha\beta}$ and $C^b_{\alpha\beta}$.

4. Algorithmic treatment

The deformation gradient $\mathbf{F} = \mathrm{Grad}\,\mathbf{x}(\mathbf{X}) = \sum_i \mathbf{g}_i \otimes \mathbf{G}^i$, with $\mathbf{g}_i$ defined by (17) in the current and $\mathbf{G}^i$ in the reference configuration, is not fully incorporated into the material law of the considered shell formulation. The penalty formulation and sequential treatment of the integration of the transversal shear terms do not accurately satisfy the Kirchhoff condition, $C_{\alpha 3} = 0$, through the thickness, and are not considered in the material equations. The deformation gradient is therefore considered here in the form

$$\mathbf{F} = \sum_\alpha \mathbf{g}_\alpha \otimes \mathbf{G}^\alpha. \tag{19}$$

To link the spin $\mathbf{w}$ (16) to the evolution of the directional axes of anisotropy $\mathbf{e}^\phi_\alpha$ the corotational rate of the axes can be considered

$$\mathring{\mathbf{e}}^\phi_\alpha = \dot{\mathbf{e}}^\phi_\alpha - \boldsymbol{\theta}^\phi \mathbf{e}^\phi_\alpha = \mathbf{0}, \tag{20}$$

(see, e.g., Dafalias, 1998). These axes of anisotropy $\mathbf{e}^\phi_\alpha$ may be updated via an incremental orthogonal transformation $\mathbf{R}_\phi$, corresponding to $\boldsymbol{\theta}^\phi \Delta t$, where $\mathbf{R}_\phi$ has to satisfy $\dot{\mathbf{R}}_\phi = \boldsymbol{\theta}^\phi \mathbf{R}_\phi$ and $\mathbf{R}_\phi(t) = \mathbf{1}$. For an application within an algorithmic treatment, $\mathbf{e}^\phi_i$ can be updated by

$${}^{t+\Delta t}\mathbf{e}^\phi_i = {}^{t+\Delta t}\mathbf{R}_\phi \, {}^t\mathbf{e}^\phi_i. \tag{21}$$

In the case of a purely elastic increment the plastic spin is identical to the zero matrix $\boldsymbol{\omega}^\phi_{\mathrm{p}} = \mathbf{0}$, and hence $\boldsymbol{\theta}^\phi = \mathbf{w} = \dot{\mathbf{R}}\mathbf{R}^{\mathrm{T}}$. Also, $\mathbf{R}_\phi$ in (21) may be identified by ${}^{t+\Delta t}\mathbf{R}_\phi = {}^{t+\Delta t}\mathbf{R}\,{}^t\mathbf{R}^{-1}$ in a total Lagrangian formulation, and simply by ${}^{t+\Delta t}\mathbf{R}_\phi = {}^{t+\Delta t}\mathbf{R}$ in an updated Lagrangian formulation. The first two columns of the right rotation tensor are therefore obtained by $\mathbf{R}_{3\times 2} = \mathbf{F}_{3\times 2}\mathbf{U}^{-1}_{2\times 2}$, where $\mathbf{U}^{-1}_{2\times 2}$ is obtained by $\mathbf{U}^2 = \mathbf{C} = \mathbf{F}^{\mathrm{T}}\mathbf{F}$. The

third term is determined by the cross-product of the first two columns, or, considering the orthogonality of $\mathbf{R}$, stated by $\mathbf{R}^{\mathrm{T}}\mathbf{R} = \mathbf{1}$. In the case of plastic loading and $\boldsymbol{\omega}_{\mathrm{p}}^{\phi} \neq \mathbf{0}$, the plastic spin $\boldsymbol{\omega}_{\mathrm{p}}^{\phi}$ also effects the update of the directional axes, and henceforward $\mathbf{R}_{\phi}$ in (21). Its algorithmic treatment will be described in the following subsections.

The anisotropic yield function ϕ is explicitly expressed with the anisotropy axes $\mathbf{e}_{\alpha}^{\phi}$. A quadratic description of the Hill (1950) yield function, for example, can be formulated as

$$\phi = \frac{1}{2}\boldsymbol{\tau}\cdot\mathbf{K}\boldsymbol{\tau}, \quad \text{where} \quad \mathbf{K} = \mathbb{K}_{\alpha\beta\delta\gamma}\mathbf{e}_{\alpha}^{\phi}\otimes\mathbf{e}_{\beta}^{\phi}\otimes\mathbf{e}_{\delta}^{\phi}\otimes\mathbf{e}_{\gamma}^{\phi} \tag{22}$$

in the plane stress state. To complete the yield criterion the isotropic hardening shall be given as

$$\bar{\sigma} = c^{\mathrm{iso}}(\bar{\varepsilon}_{\mathrm{o}} + \bar{\varepsilon}_{\mathrm{p}})^{n^{\mathrm{iso}}}, \tag{23}$$

with $\bar{\varepsilon}_{\mathrm{o}}$, c^{iso} and n^{iso} being material parameters. $\bar{\sigma}$ and $\bar{\varepsilon}_{\mathrm{o}}$ shall be called the equivalent yield stress and the initial strain to yield, respectively. In the chosen notation (q, α) for the isotropic hardening $\bar{\sigma}$ can be identified with q and $\dot{\bar{\varepsilon}}_{\mathrm{p}}$ with $\dot{s} = \sqrt{\frac{2}{3}}\|\mathbf{d}_{\mathrm{p}}\|$.

Stress update algorithm. Because the plane stress condition is assumed the stress and strain tensors can be defined in a 2×2 vector space. As a starting point the incremental deformation gradient $\mathbf{F}$—mapping $\mathscr{B}_n$ to $\mathscr{B}_{n+1}$—, the strain increments $\Delta\boldsymbol{\varepsilon} = \mathbf{d}\Delta t$, and the variables $\boldsymbol{\tau}^n$, $\boldsymbol{\varepsilon}_{\mathrm{p}}^n$, $\bar{\varepsilon}_{\mathrm{p}}^n$, $\mathbf{e}_{\alpha}^{\phi^n}$ from the previous load step n are assumed to be given.

It is first assumed that no plastic loading is present. Therefore $\Delta\boldsymbol{\varepsilon}_{\mathrm{p}} = \mathbf{d}_{\mathrm{p}}\Delta t = \mathbf{0}$ and $\overset{\Delta}{\boldsymbol{\omega}}{}_{\mathrm{p}}^{\phi} = \boldsymbol{\omega}_{\mathrm{p}}^{\phi}\Delta t = \mathbf{0}$ are valid yielding the relations $\overset{\Delta}{\boldsymbol{\theta}}{}^{\phi} = \boldsymbol{\theta}^{\phi}\Delta t = \mathbf{w}\Delta t = \overset{\Delta}{\mathbf{w}}$. With (21) the directional axes of the yield function ϕ are updated with an orthogonal transformation $\mathbf{R}_{\phi}$ corresponding to $\overset{\Delta}{\boldsymbol{\theta}}{}^{\phi}$

$$\mathbf{e}_i^{\phi^{\mathrm{trial}}} = \mathbf{R}_{\phi}^{\mathrm{trial}}\mathbf{e}_i^{\phi^n}, \tag{24}$$

which defines the trial orientation for the anisotropic yield function. Thereby $\mathbf{R}_{\phi}^{\mathrm{trial}}$ is defined with $\mathbf{R}_{\phi}^{\mathrm{trial}} = \mathbf{R}$ in an updated Lagrangian setting.

For the stress update algorithm, within a time increment with fixed directional axes, we consider the stresses to be given at the time or load step n, and the total strain increment at loadstep $n+1$. To be determined are the stresses $\boldsymbol{\tau}$ and the plastic strain increment $\Delta\boldsymbol{\varepsilon}_{\mathrm{p}}$ at $n+1$. The stresses at $n+1$ can be written as

$$\boldsymbol{\tau}^{n+1} = \mathbf{F}\boldsymbol{\tau}^n\mathbf{F}^{\mathrm{T}} + \Delta\boldsymbol{\tau}^{n+1}, \tag{25}$$

which correlates to the Oldroyd derivative for stress like variables $(.)^{\nabla} = (.) - \mathbf{1}\dot{(.)} - (.)\mathbf{1}^{\mathbf{T}}$, identical to the Lie-derivative defined as $L_v(.) = \mathbf{F}[\frac{\partial}{\partial t}(.)]\mathbf{F}^{\mathrm{T}}$ in an updated Lagrangian setting (see Simo and Hughes, 1998; Oldroyd, 1950). With $\Delta\boldsymbol{\varepsilon} = \mathbf{d}\Delta t$ the stress increment yields

$$\Delta\boldsymbol{\tau} = \mathbb{C}_{\mathrm{e}}(\Delta\boldsymbol{\varepsilon} - \Delta\boldsymbol{\varepsilon}_{\mathrm{p}}), \tag{26}$$

where $\Delta\boldsymbol{\varepsilon}$ is described in Simo and Hughes (1998) as $\Delta\boldsymbol{\varepsilon} = \mathbf{e} = (1/2)(\mathbf{1} - \mathbf{F}^{-\mathrm{T}}\mathbf{F}^{-1})$ identical to the incremental Almansi strain tensor. By setting $\Delta\boldsymbol{\varepsilon}_{\mathrm{p}}^{\mathrm{trial}} = \mathbf{0}$ the trial stress increments are obtained as

$$\Delta\boldsymbol{\tau}^{\mathrm{trial}} = \mathbb{C}_{\mathrm{e}}\,\Delta\boldsymbol{\varepsilon} \tag{27}$$

or, equivalently, the total trial stresses as $\boldsymbol{\tau}^{\mathrm{trial}} = \mathbf{F}\boldsymbol{\tau}^n\mathbf{F}^{\mathrm{T}} + \mathbb{C}_{\mathrm{e}}\Delta\boldsymbol{\varepsilon}^{n+1}$. The trial value for the stress-like internal variable describing the isotropic hardening are set to

$$q^{\mathrm{trial}} = q^n. \tag{28}$$

The constitutive equations are performed in the plane stress state defined in the tangential coordinate system of the shell. In order to remain in a two-dimensional coordinate system it may be helpful to formulate the relation (25) relative to the referential coordinate system $\mathbf{e}_\alpha^{\phi^n}$, written as

$$\hat{\boldsymbol{\tau}}^{n+1} = \mathbf{U}\boldsymbol{\tau}^n\mathbf{U}^{\mathrm{T}} + \Delta\hat{\boldsymbol{\tau}}^{n+1}. \tag{29}$$

The stress tensor in the current basis $\mathbf{e}_\alpha^{\phi^{n+1}}$ is then recovered by $\boldsymbol{\tau} = \mathbf{R}\hat{\boldsymbol{\tau}}\mathbf{R}^{\mathrm{T}}$. The coefficients of the tensor $\boldsymbol{\tau}$, however, do not change if the basis is corotated with the deformation (see Bathe, 1996; Yoon et al., 1999, or Han et al., submitted). Correspondingly,

$$\Delta\hat{\boldsymbol{\varepsilon}} = \mathbf{R}^{\mathrm{T}}\Delta\boldsymbol{\varepsilon}\mathbf{R} = \tfrac{1}{2}(\mathbf{1} - \mathbf{C}^{-1}) \tag{30}$$

is obtained for the strain increments and (26) and (27) remain valid if $\boldsymbol{\tau}$ and $\boldsymbol{\varepsilon}$ are understood in the sense of a matrix notation.

(E) *Elastic loading*. If the yield condition is fulfilled with these trial values

$$\Phi^{\mathrm{trial}} = \Phi(\boldsymbol{\tau}^{\mathrm{trial}}, q^{\mathrm{trial}}; \mathbf{e}_\alpha^{\phi^{\mathrm{trial}}}) \leqslant \mathrm{tol} \tag{31}$$

the load step $n+1$ is considered to be elastic and hence $\mathbf{d}_{\mathrm{p}} = \boldsymbol{\omega}_{\mathrm{p}}^{\phi} = \mathbf{0}$ and

$$\boldsymbol{\tau}^{n+1} = \boldsymbol{\tau}^{\mathrm{trial}}, \quad q^{n+1} = q^{\mathrm{trial}}, \quad \mathbf{e}_\alpha^{\phi^{n+1}} = \mathbf{e}_\alpha^{\phi^{\mathrm{trial}}} \tag{32}$$

and we can proceed to the next load step $n+2$. Otherwise, if the tolerance is exceeded in (31) we continue with the following step **(P)**.

(P) *Plastic loading*. In the case of plastic loading $\Phi^{\mathrm{trial}} \geqslant 0$ the plastic strain increments are obtained by projection of the trial stresses to the current yield surface by

$$\boldsymbol{\tau} = \boldsymbol{\tau}^{\mathrm{trial}} - \mathbb{C}_{\mathrm{e}}\,\Delta\boldsymbol{\varepsilon}_{\mathrm{p}}. \tag{33}$$

This projection is approached incrementally, and for each iteration state i the plastic increments are defined by the incremental form of the associated flow rule

$$\Delta\boldsymbol{\varepsilon}_{\mathrm{p}}^i = \Delta\gamma^i \frac{\partial\phi^i}{\partial\boldsymbol{\tau}} \tag{34}$$

and by the corresponding increments of the isotropic hardening

$$\Delta q^i = \Delta\gamma^i n^{\mathrm{iso}} c^{\mathrm{iso}} (\bar{\varepsilon}_{\mathrm{o}} + \bar{\varepsilon}_{\mathrm{p}}^i)^{n^{\mathrm{iso}}-1} \left| \frac{\partial\phi^i}{\partial\boldsymbol{\tau}} \right|. \tag{35}$$

With $q^i = q^{\mathrm{trial}} + \Delta q^i$ all stress-like variables $\boldsymbol{\tau}$ and q are now expressed in terms of $\Delta\gamma$. Thus $\Delta\gamma$ can be determined solving the condition

$$\Phi(\boldsymbol{\tau}(\Delta\gamma), q(\Delta\gamma)) = 0, \tag{36}$$

with a Newton iteration $\Delta\gamma^{i+1} = \Delta\gamma^i - \Phi^i/(\partial\Phi^i/\partial\Delta\gamma)$. Herein Φ^i is expressed with q^i and $\mathbf{K}^i = \mathbb{K}_{\alpha\beta\delta\gamma}\mathbf{e}_\alpha^{\phi^i} \otimes \mathbf{e}_\beta^{\phi^i} \otimes \mathbf{e}_\delta^{\phi^i} \otimes \mathbf{e}_\gamma^{\phi^i}$. Details of the derivation $(\partial\Phi/\partial\Delta\gamma)$ may not be trivial but are straightforward and omitted here for brevity. Missing, however, is a description of how $\mathbf{e}_\beta^{\phi^i}$ is updated. This will be shown in the following under **(U)**.

(U) *Update of* $\mathbf{e}_\beta^{\phi^i}$. The directional axes of the yield function rotate in general according to $\boldsymbol{\theta}^{\phi} = \mathbf{w} - \boldsymbol{\omega}_{\mathrm{p}}^{\phi}$ and (21). An incremental form can be written as

$$\overset{\Delta}{\boldsymbol{\theta}}{}^{\phi} = \overset{\Delta}{\mathbf{w}} - \overset{\Delta}{\boldsymbol{\omega}}{}_{\mathrm{p}}^{\phi}, \tag{37}$$

where the increments of the plastic spin can be expressed with the incremental plastic strains as

$$\overset{\Delta}{\boldsymbol{\omega}}{}_{\mathrm{p}}^{\phi} = \mu^{\phi}(\boldsymbol{\tau}\Delta\boldsymbol{\varepsilon}_{\mathrm{p}} - \Delta\boldsymbol{\varepsilon}_{\mathrm{p}}\boldsymbol{\tau}) \tag{38}$$

and the increments of the material spin tensor $\mathbf{w}$ are determined by the increments of the velocity gradient $\mathbf{l} = \dot{\mathbf{F}}\mathbf{F}^{-1}$ as $\overset{\Delta}{\mathbf{l}} = \mathbf{l}\Delta t \approx \Delta\mathbf{F}\mathbf{F}^{-1} = (\mathbf{F} - \mathbf{1})\mathbf{F}^{-1} = \mathbf{1} - \mathbf{F}^{-1}$. This yields the increments in the material spin $\overset{\Delta}{\mathbf{w}} = (1/2)(\overset{\Delta}{\mathbf{l}} - \overset{\Delta}{\mathbf{l}}{}^{\mathrm{T}})$. To each of the increments $\overset{\Delta}{\mathbf{w}}$, $\overset{\Delta}{\boldsymbol{\omega}}{}_{\mathrm{p}}^{\phi}$, and $\overset{\Delta}{\boldsymbol{\theta}}{}^{\phi}$ the rotation tensors $\mathbf{R}$, $\mathbf{R}_{\omega^{\phi}}$, and $\mathbf{R}_{\phi}$, can be introduced, and their relation to each other is then formed by subsequent rotations

$$\mathbf{R}_{\phi} = \mathbf{R}_{\omega^{\phi}}^{\mathrm{T}}\mathbf{R}. \tag{39}$$

The material rotation $\mathbf{R}$ is already contained in $\mathbf{e}_{\alpha}^{\phi^{\mathrm{trial}}} = \mathbf{R}\mathbf{e}_{\alpha}^{\phi^{n}}$. The rotation remaining in the elasto-plastic routine is applied by the inplane rotation $\mathbf{R}_{\omega^{\phi}}$ within the tangential plane, where the constitutive equations are defined as

$$\mathbf{e}_{\alpha}^{\phi^{n+1}} = \mathbf{R}_{\omega^{\phi}}^{\mathrm{T}}\mathbf{e}_{\alpha}^{\phi^{\mathrm{trial}}}, \quad \alpha = 1, 2 \tag{40}$$

and the third direction remains unchanged.

The algorithmic steps are summarized in Table 4 for clarity.

Remark. Relation (39) can be easily verified in the planar case. The axes of anisotropy $\mathbf{e}_{\alpha}^{\phi}$ are updated by an orthogonal transformation $\mathbf{R}_{\phi}$, corresponding to $\boldsymbol{\theta}^{\phi}\Delta t$. For the determination of this rotational tensor we consider the following expression of (20)

$$\begin{bmatrix} -\sin\vartheta \\ \cos\vartheta \end{bmatrix}\dot{\vartheta} - \theta_{12}^{\phi}\begin{bmatrix} 0 & 1 \\ -1 & 0 \end{bmatrix}\begin{bmatrix} \cos\vartheta \\ \sin\vartheta \end{bmatrix} = \begin{bmatrix} 0 \\ 0 \end{bmatrix}, \tag{41}$$

where $\mathbf{e}_{\alpha}^{\phi}$ shall be determined with the angle ϑ. Eq. (41) yields $\dot{\vartheta} = -\theta_{12}^{\phi}$ and, henceforward with $\Delta\vartheta = -\overset{\Delta}{\theta}{}_{12}^{\phi}$, the rotation

Table 4
Algorithmic steps

Input: $\mathbf{F}$, $\boldsymbol{\tau}^{n}$, $\bar{\varepsilon}_{\mathrm{p}}^{n}$, $\mathbf{e}_{\alpha}^{\phi^{n}}$
- Compute $\Delta\boldsymbol{\varepsilon}^{n+1}$, $\boldsymbol{\tau}^{\mathrm{trial}}$, $\mathbf{e}_{\alpha}^{\phi^{\mathrm{trial}}}$
- Evaluate Φ with $\mathbf{K}^{\mathrm{trial}} = \mathbb{K}_{\alpha\beta\delta\gamma}\mathbf{e}_{\alpha}^{\phi^{\mathrm{trial}}} \otimes \mathbf{e}_{\beta}^{\phi^{\mathrm{trial}}} \otimes \mathbf{e}_{\delta}^{\phi^{\mathrm{trial}}} \otimes \mathbf{e}_{\gamma}^{\phi^{\mathrm{trial}}}$

(**E**) if $\Phi < tol$ then
$\boldsymbol{\tau}^{n+1} = \boldsymbol{\tau}^{\mathrm{trial}}$, $\bar{\varepsilon}_{\mathrm{p}}^{n+1} = \bar{\varepsilon}_{\mathrm{p}}^{n}$, $\mathbf{e}_{\alpha}^{\phi^{n+1}} = \mathbf{e}_{\alpha}^{\mathrm{trial}}$

(**P**) elseif $\Phi \geqslant tol$ then
$\mathbf{K}^{0} = \mathbf{K}^{\mathrm{trial}}$, $\Delta\gamma^{0} = 0$, $\boldsymbol{\tau}^{0} = \boldsymbol{\tau}^{\mathrm{trial}}$, $\Delta\boldsymbol{\varepsilon}_{\mathrm{p}}^{0}$, Φ^{0}
do $i = 0$, $i_{\max}$
compute
- $\frac{\partial\Phi^{i}}{\partial\Delta\gamma_{i}}$
- $\Delta\gamma^{i+1} = \Delta\gamma^{i} - \Phi^{i}/\frac{\partial\Phi^{i}}{\partial\Delta\gamma}$
- $\boldsymbol{\tau}^{i+1}$, $\Delta\boldsymbol{\varepsilon}_{\mathrm{p}}^{i+1}$ via (33), (34), and $\Delta\bar{\varepsilon}_{\mathrm{p}}^{i+1}$
- $\mathbf{R}_{\omega^{\phi}}$ via (38)
- $\mathbf{e}_{\alpha}^{\phi^{i+1}} = \mathbf{R}_{\omega^{\phi}}\mathbf{e}_{\alpha}^{\mathrm{trial}}$
- $\mathbf{K}^{i+1}$
- Φ^{i+1}
- if $\Phi^{i+1} < tol$ then
$\boldsymbol{\tau}^{n+1} = \boldsymbol{\tau}^{i+1}$, $\bar{\varepsilon}_{\mathrm{p}}^{n+1} = \bar{\varepsilon}_{\mathrm{p}}^{i+1}$, $\mathbf{e}_{\alpha}^{\phi^{n+1}} = \mathbf{e}_{\alpha}^{\phi^{i+1}}$
return
end if

enddo

Output: $\boldsymbol{\tau}^{n+1}$, $\bar{\varepsilon}_{\mathrm{p}}^{n+1}$, $\mathbf{e}_{\alpha}^{\phi^{n+1}}$

$$\mathbf{R} = \begin{bmatrix} \cos\Delta\vartheta & -\sin\Delta\vartheta \\ \sin\Delta\vartheta & \cos\Delta\vartheta \end{bmatrix} = \mathbf{R}_\phi^{\mathrm{T}} \tag{42}$$

is obtained. All antisymmetric tensors can be expressed as $\mathbf{R}_\phi$ in (41) which yields with (38), $\overset{\Delta}{\theta}{}^{\phi}{}_{12} = \overset{\Delta}{w}{}^{12} - \overset{\Delta}{\omega}{}^{\phi}{}_{p12}$. Proper orthogonal tensors can be represented in the 2D case by (42) and an additive relation of rotation angles results in a multiplicative relation by trigonometric transformations.

5. Numerical examples

5.1. Uniaxial stretching

To assess the performance of the derived stress-update algorithm the uniaxial stretch tests investigated in Dafalias (2000) and Kim and Yin (1997) are considered. Rectangular samples are cut from a larger sheet in the angles 30°, 45°, and 60° from the rolling direction, and stretched along these directions. An analytical solution for rigid-plastic material, incorporating plastic spin and Hill's yield function without any hardening, is presented in Dafalias (2000).

The material parameters used for the simulation with the proposed algorithm are taken from the prestretched mild steel described in Kim and Yin (1997), and are given in Table 5. The definition of Hill's yield function is thereby described via

$$\Phi = \sqrt{\boldsymbol{\tau}\cdot\mathbf{K}\boldsymbol{\tau}} - \sqrt{2/3}q, \tag{43}$$

where $\boldsymbol{\tau}$ and $\mathbf{K}$ are understood as matrices defined as

$$\boldsymbol{\tau} = \begin{bmatrix} \tau_{11} \\ \tau_{22} \\ \tau_{12} \end{bmatrix} \quad \text{and} \quad \mathbf{K} = \frac{2}{3}\begin{bmatrix} 1 & -\beta_{12} & 0 \\ -\beta_{12} & \beta_{22} & 0 \\ 0 & 0 & \beta_{66} \end{bmatrix}, \tag{44}$$

with respect to the anisotropy directions $\mathbf{e}_\alpha^\phi$.

Tensile stretch tests of strips cut from a large sheet in the angles 30°, 45°, and 60° to the rolling direction are considered to compare their results of the experiments (Kim and Yin, 1997), the analytical solution (Dafalias, 2000), and the algorithm are compared in Fig. 3, where about 2200 time steps have been applied for the algorithmic solution. These and all following simulations are performed with explicit FEM algorithms. The results of the analytical and algorithmic solutions are shown for different values of c_K, namely −100, −200 and −300. Because the material model of the algorithm also incorporates elastic strains, the results of the algorithmic and the analytical solution cannot be identical, a priori. But, as can be seen in Fig. 3, there are only minor differences between these solutions.

For the angles 30° and 60° a value of $c_K = -100$ to −200 in (12) would fit the experimental best, for the angle 45°, however, a value of $c_K = -300$ would be more appropriate. To obtain a better agreement with the experimental data with one single parameter for all three cases a simple modification of μ^ϕ in (12) is suggested by introducing the minimum angle $\vartheta \in [0°, 45°]$ between any of the anisotropy axes $\mathbf{e}_\alpha^\phi$ and the

Table 5
Material parameters

Young's modulus	$E = 206$ GPa
Poisson's ratio	$\nu = 0.3$
Initial yield stress	$\tau_o = 107.06$ MPa
Hill's 1950 yield function	$\beta_{12} = 0.58373$, $\beta_{22} = 1.00919$, $\beta_{66} = 2.3550$
Isotropic hardening	$c_{iso} = 544$ MPa, $n_{iso} = 0.25$

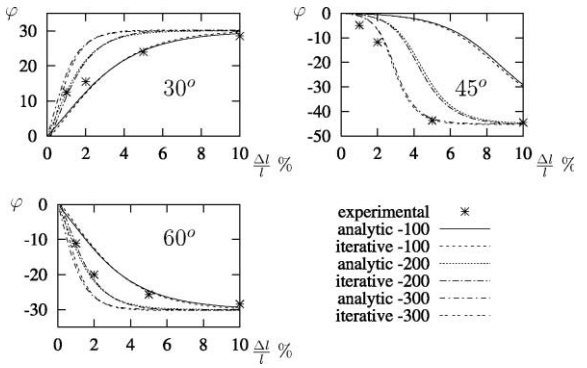

Fig. 3. Rotation angle φ between $\mathbf{e}^{\phi}_{o_\alpha}$ and $\mathbf{e}^{\phi}_{\alpha}$ (see Fig. 1) versus strain using (12) with $c_K = -100$, -200, and -300.

principal axes $\mathbf{n}^{\alpha}_{\mathrm{p}}$ of the rate of deformation tensor $\mathbf{d}_{\mathrm{p}} = \sum_{\alpha} \dot{\lambda}^{\alpha}_{\mathrm{p}} \mathbf{n}^{\alpha}_{\mathrm{p}} \otimes \mathbf{n}^{\alpha}_{\mathrm{p}}$. With this angle the spin description (12) is modified to

$$\mu^{\phi} = \frac{c^{\phi}}{\phi} \tan(\vartheta). \tag{45}$$

With this description (45) of μ^{ϕ} the anisotropy axes of the strip cut in an angle of 45° from RD will spin with the same rotation rate as the strip cut in the angle of 30° after the anisotropy axes of the 45° sample are parallel to those of the 30° sample in its initial state. The results of this approach for the tensile stretch test in the directions 30°, 45°, and 60° are presented in Fig. 4 using one single material parameter $c^{\phi} = -350$.

In Fig. 5 the flow stress obtained by $\boldsymbol{\omega}^{\phi} = \mathbf{0}$ and the descriptions denoted in (12) with $c_K = -100$ as suggested in Kuroda and Tvergaard (2000) and (45) with $c^{\phi} = -350$ are presented. Only the calculations for the angles 0°, 30°, and 45° are illustrated, the results for 60° and 90° are almost identical to 30° and 0° since β_{22} is with its value 1.00919 very close to $\beta_{11} = 1.0$. As can be seen in Fig. 5 the differences between the description (12) and (45) are of some significance for strains of 0.015–0.005. For larger strains the differences are rather minor. The differences in the flow stresses with or without a spin description are, however, of considerable magnitude. For processes where the loading direction is frequently changed a good agreement of the anisotropy directions in the deformation process could be of importance. In this regard it should be noted that by using additional parameters in (45), e.g., $\mu^{\phi} = (c^{\phi}/\phi)\{\tan^{n_1}(\vartheta) + n_2\}$, an even better fit of the experimental data could be achieved.

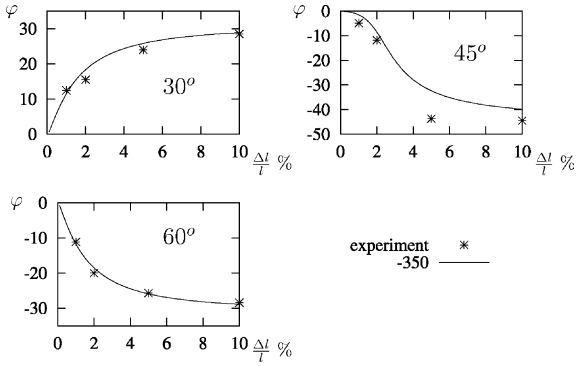

Fig. 4. Rotation angle φ between $\mathbf{e}^{\phi}_{o_\alpha}$ and $\mathbf{e}^{\phi}_{\alpha}$ versus strain using (45) with $c^{\phi} = -350$.

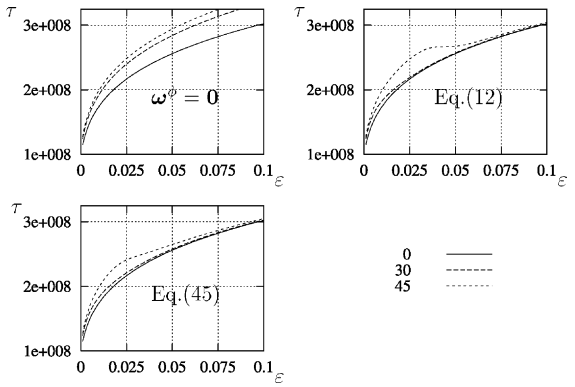

Fig. 5. Flow stress with $\boldsymbol{\omega}^{\phi} = \mathbf{0}$, (12) with $c_K = -100$, and (45) with $c^{\phi} = -350$.

5.2. Square Cup drawing

For simulation of an applied problem, the Square Cup drawing benchmark of NUMISHEET'93 (Makinouchi et al., 1993) is considered. An initially square blank, with dimensions of 150 mm by 150 mm and a thickness of 0.9 mm, is formed by the usual punch, die and blankholder constellation. All tools are modeled as rigid surfaces. The edge-length of the punch is 70 mm and rounded at the corners with a radius of 10 mm. The geometry of the die is defined by a square hole, 74 mm by 74 mm, also rounded at the corners with a radius of 12 mm. The vertical blankholder force is given as 1.75 KN and the friction between the sheet and die, and sheet and punch, is $\mu = 0.1$. The punch is moved to $U_{\text{punch}} = 24$ mm after the first contact with the sheet. As plastic spin parameter $c^{\phi} = -350$ is chosen as before. For comparison, the results of the simulation without plastic spin are also shown. The rolling direction is assumed to be parallel to one edge of the sheet. The symmetry conditions are still valid for this problem because the plastic spin can be considered to be zero along the lines of symmetry. Only a quarter of the structure is thus discretized with 50×50 elements and 25 integration points through the thickness are applied.

The punch load versus punch travel is shown in Fig. 6 (left). The forces needed for the punch travel with plastic spin are about 10–15% smaller in the final load steps. The contours of the deformed sheet are, however, about the same (see Fig. 6 (right)). This should not be surprising, because the deformation is mainly controlled by the punch travel which allows little space for variations. As can been seen in Fig. 7, where the equivalent plastic strain $\bar{\varepsilon}_{\text{p}}$ of the simulations with and without plastic spin are plotted, the differences in $\bar{\varepsilon}_{\text{p}}$ are rather minor. While there is little differences in the deformation of the sheet the differences in the stresses, however, are worth noticing. The von Mises stresses, presented in Fig. 8, with plastic

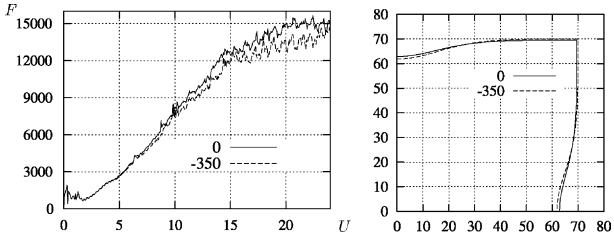

Fig. 6. Punch force versus punch travel (left) and contours of the deformed sheet (right) for the spin descriptions $\boldsymbol{\omega}^{\phi} = \mathbf{0}$ and (45) with $c^{\phi} = -350$ of the Square Cup.

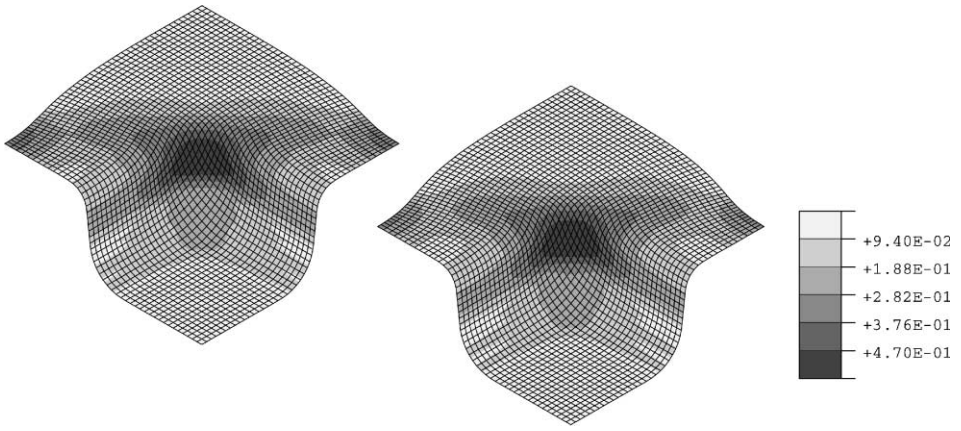

Fig. 7. Equivalent plastic strains without (left) and with plastic spin (right) of the Square Cup.

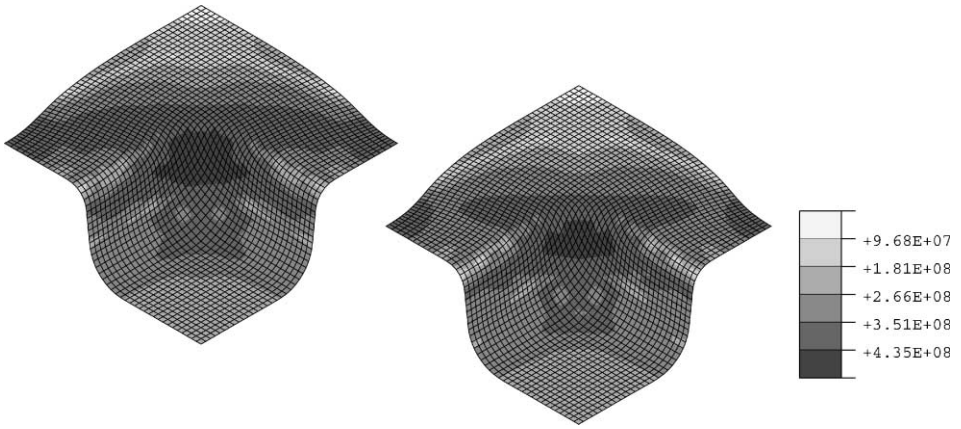

Fig. 8. Von Mises stresses without (left) and with spin (right) of the Square Cup.

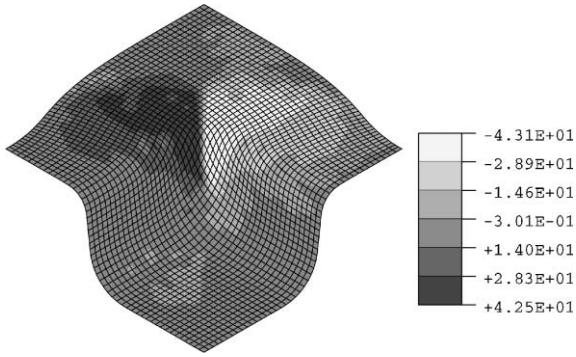

Fig. 9. Rotation angles between $\mathbf{e}^{\phi}_{\mathrm{o}_\alpha}$ and $\mathbf{e}^{\phi}_{\alpha}$ of the Square Cup (material rotations are not included).

spin are of lower magnitude than without plastic spin yielding the lower punch forces in Fig. 6 (left). These lower stresses are caused by the rotation of the anisotropy directions, shown in Fig. 9, as it was also shown

for the stretch test in Fig. 5. These rotations reach maximal values of over $\pm 40°$ and are located close to the diagonal of the sheet.

5.3. Wrinkling of a Cylindrical Cup

In another sheet forming example the wrinkling and earing behavior shall be investigated. The geometry of the tools are considered in the NUMISHEET 2002 benchmark (Fig. 10) where the punch has a radius of 50 mm and is rounded at the edge with a radius of 9.5 mm, the radius of the die opening is 51.25 mm and rounded at the die opening with a radius of 7 mm. The punch stroke is given as 40 mm and the blank holder force as 800 N. The sheet is of circular shape with a radius of 105 mm. The Coulomb friction with the coefficient $\mu = 0.15$ between the sheet and tools is applied. As sheet material the same material as in the previous examples were applied. The spin description (45) is used. As in the previous example only a quarter of the sheet is discretized with the edges along the rolling and transverse direction. The FE mesh contains 2104 elements.

The vertical displacements in mm and outer contour of the simulations in the final stage are presented in Fig. 11. The amplitudes (the gap between die and blankholder without spin is 1.116 mm versus 0.951 mm with spin) of the wrinkles are less pronounced with plastic spin and the higher frequency of the wrinkles is higher with plastic spin. The earing effect is smaller with plastic spin as can be also seen in Table 6 where the draw-in in the angles 0°, 45°, and 90° from the rolling direction is given. In this example the rotation of the anisotropy axes (Fig. 12) gradually effects the flow stress in radial direction to approach the flow stresses in rolling and transverse direction which can be also seen from the flow stresses of the tensile tests in Fig. 5. The anisotropic deformation of this problem simulated with plastic spin is therefore less pronounced then

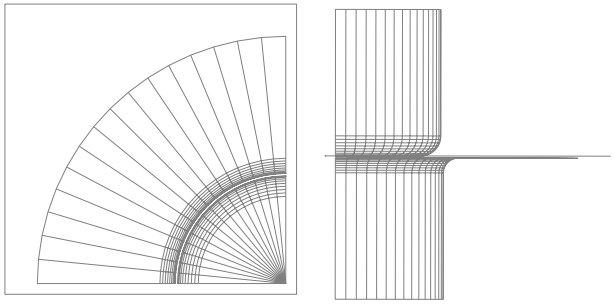

Fig. 10. Tools of the Cylindrical Cup.

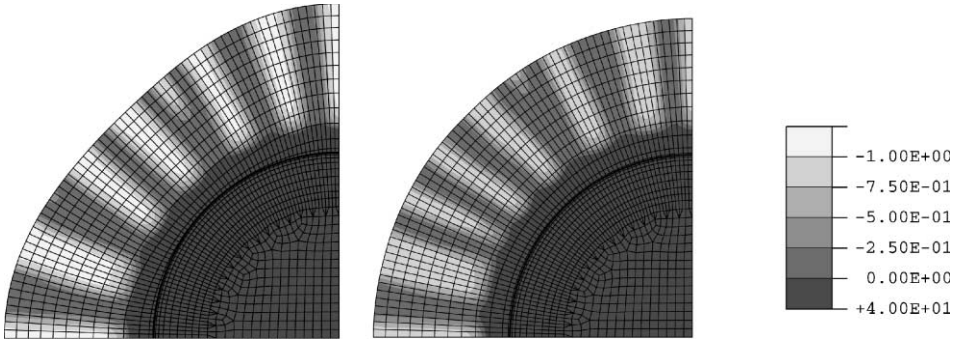

Fig. 11. Vertical displacements (in mm) and contour of the Cylindrical Cup without (left) and with plastic spin (right).

Table 6
Draw-in of the sheet

Angle from RD	0°	45°	90°
Draw-in without plastic spin (mm)	13.81	20.21	13.77
Draw-in with plastic spin (mm)	16.77	17.41	16.72

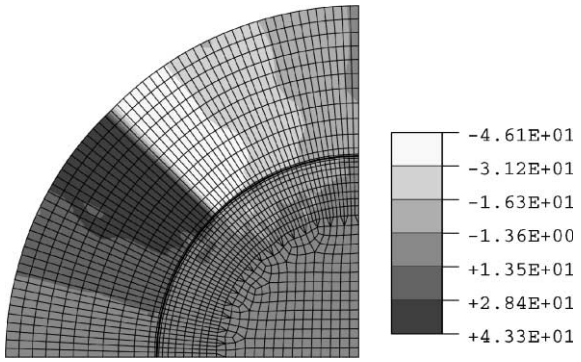

Fig. 12. Rotation angles of the Cylindrical Cup.

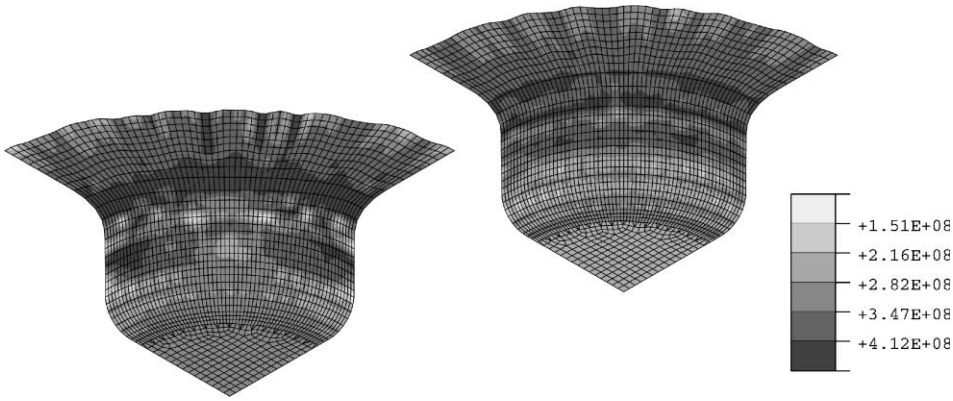

Fig. 13. Von Mises stresses without (left) and with plastic spin (right) of the Cylindrical Cup.

without. Correspondingly, the stresses in the circumferential direction show less variation with plastic spin (Fig. 13, right) than without (Fig. 13, left).

6. Conclusions

A relatively simple, but thermodynamically consistent, numerical treatment for the planar elasto-plastic materials at large strains has been proposed, incorporating the plastic spin to describe the evolution of the anisotropy directions. The spin formulation of Kuroda (1997) has thereby been modified to obtain a better agreement with the experimental results of Kim and Yin (1997). Other common yield functions, like the Barlat et al. (1991, 1997) yield functions used for the simulation of thin-walled elasto-plastic structures, can

be easily incorporated in the presented numerical treatment. The assumption that the orthogonality of the anisotropy axes is preserved, however, is a necessary basis of this approach.

Although the differences—resulting from applying the plastic spin or not—in the deformation of the second example are of minor magnitude, the differences in the stresses are worth noting. These differences in the stresses are caused by rotations of the anisotropic directions defining the elastic boundaries. Thus, the deformed shape of the sheet will also result in a different structural response, particularly if the sensitive springback behavior is considered, whether or not the plastic spin is used. A proper description of the springback behavior (see Li et al., 1999; Geng et al., 2002 or Chun et al., 2002a), is considered to be essential for a reliable prediction of the final shape of the sheet. Such predictions are preferably performed with implicit algorithms and are not performed here. That the plastic spin can also affect the deformed shape has been illustrated with the third example where the material spin/rotation can be almost neglected. Considerable differences in wrinkling performance and earing behavior have been simulated.

Though the rotation of the anisotropy axes seems experimentally and theoretically well established, the magnitude and the micromechanical origin of the different spin rates for aluminum and mild steel, however, still pose open questions. Further investigations on the magnitude of the plastic spin would be also necessary for other metallic polycrystal and high strength steel which may as aluminum exhibit a different behavior than mild steel. Within hydroforming and multi-stage forming processes (e.g., Chun et al., 2002b), strains over 80% can be obtained. For such large strains the low rotation rates of 5° at 20% observed in Bunge and Nielsen (1997) and Truong Qui and Lippmann (2001) would effect the material behavior considerably. At these high strains the assumption used here that the strains inducing the anisotropy of the pre-existing preferred orientation is much larger than subsequent strains due to further deformation is not valid. The symmetry planes may not be orthogonal anymore, the evolution of microstructures, like dislocation walls and cells, may influence the shape of the yield function considerably, and the texture evolution and thus the evolution of the anisotropy properties at such high strains will affect the anisotropic properties not only in terms of rotations of the symmetry planes but also in terms of the yield surface shape. The avail of the presented spin approach for such processes has still to be verified at such high strains.

Acknowledgements

The financial support of the National Science Foundation (DMR 0139045) and the Center for Advanced Materials and Manufacturing of Automotive Components (CAMMAC) is gratefully acknowledged. Computer resources were provided by The Ohio Supercomputer Center (PAS 080).

References

Asaro, R.J., 1983. Micromechanics of crystals and polycrystals. Adv. Appl. Mech. 23, 1–115.

Barlat, F., Lege, D.J., Brem, J.C., 1991. A six-component yield function for anisotropic materials. Int. J. Plast. 7, 693–712.

Barlat, F., Maeda, Y., Chung, K., Yanagawa, M., Brem, J.C., Hayashida, Y., Lege, D.J., Matsui, K., Murtha, S.J., Hattori, S., Becker, R.C., Makosey, S., 1997. Yield function development for aluminum alloy sheets. J. Mech. Phys. Solids 45, 1727–1763.

Bathe, K.-J., 1996. Finite Element Procedures. Prentice-Hall.

Boehler, J.P., Koss, S., 1991. Evolution of anisotropy in sheet-steels subjected to off-axes large deformation. In: Brueller, O., Mannl, V., Najar, J. (Eds.), Advances in Continuum Mechanics. Springer, pp. 143–158.

Boyce, M.C., Weber, G.G., Parks, D.M., 1989. On the kinematics of finite strain plasticity. J. Mech. Phys. Solids 37, 647–665.

Bunge, H.J., 1982. Texture Analysis in Material Science. Butterworths.

Bunge, H.J., Nielsen, I., 1997. Experimental determination of plastic spin in polycrystalline materials. Int. J. Plast. 13, 435–446.

Chun, B.K., Jinn, J.T., Lee, J.K., 2002a. Modeling the Bauschinger effect for sheet metals, part I: Theory. Int. J. Plast. 18, 571–595.

Chun, B.K., Kim, H.Y., Lee, J.K., 2002b. Modeling the Bauschinger effect for sheet metals, part II: Applications. Int. J. Plast. 18, 597–616.

Chung, K., Shah, K., 1992. Finite element simulation of sheet metal forming for planar anisotropic metals. Int. J. Plast. 8, 453–476.
Dafalias, Y.F., 1985. The plastic spin. J. Appl. Mech. 52, 865–871.
Dafalias, Y.F., 1998. Plastic spin: necessity or redundancy. Int. J. Plast. 14, 909–931.
Dafalias, Y.F., 2000. Oriental evolution of plastic orthotropy in sheet metals. J. Mech. Phys. Solids 48, 2231–2255.
Eberlein, R., Wriggers, P., 1999. Finite element concepts for finite elastoplastic strains and isotropic stress response in shells: theoretical and computational analysis. Comp. Meth. Appl. Mech. Eng. 171, 234–279.
Geng, L., Shen, Y., Wagoner, R.H., 2002. Anisotropic hardening equations derived from reverse-bend testing. Int. J. Plast. 18, 743–767.
Han, C.S., Chung, K., Wagoner, R.H., Oh, S.I., in press. An anisotropic finite elastoplastic formulation with a multiplicative decomposition of the deformation gradient. Int. J. Plast.
Han, C.S., Lee, M.G., Chung, K., Wagoner, R.H., submitted. Integration algorithms for planar anisotropic shells with isotropic and kinematic hardening at finite strains.
Han, C.S., Wriggers, P., 2000. An h-adaptive method for elasto-plastic shell problems. Comp. Meth. Appl. Mech. Eng. 189, 651–671.
Haupt, P., Tsakmakis, C., 1986. On kinematic hardening and large plastic deformations. Int. J. Plast. 2, 279–293.
Hauptmann, R., Schweizerhof, K., 1998. A systematic development of 'solid-shell' element formulation for linear and non-linear analysis employing only displacement degrees of freedom. Int. J. Numer. Meth. Eng. 42, 49–69.
Hill, R., 1950. The Mathematical Theory of Plasticity. Oxford University Press.
Kim, K.H., Yin, J.J., 1997. Evolution of anisotropy under plane stress. J. Mech. Phys. Solids 45, 841–851.
Kuroda, M., 1997. Interpretation of the behavior of metals under large plastic shear deformations: a macroscopic approach. Int. J. Plast. 13 (4), 359–383.
Kuroda, M., Tvergaard, V., 2000. Forming limit diagrams for anisotropic metal sheets with different yield criteria. Int. J. Solid Struct. 37, 5037–5059.
Lee, E.H., 1969. Elastic–plastic deformations at finite strains. J. Appl. Mech. 36, 1.
Lee, H., Im, S., Atluri, S.N., 1995. Strain localization in an orthotropic material with plastic spin. Int. J. Plast. 11, 423–450.
Levitas, V.I., 1998. A new look at the problem of plastic spin based on stability analysis. J. Mech. Phys. Solids 46 (3), 557–590.
Li, K.P., Geng, L.M., Wagoner, R.H., 1999. Simulation of springback with the draw/bend test. In: Meech et al. (Eds.), IPMM '99. IEEE, Vancouver, BC, Canada, ISBN 0-7803-5489-3.
Loret, B., 1983. On the effects of plastic rotation in the finite deformation of anisotropic elastoplastic materials. Mech. Mater. 2, 287–304.
Lubarda, V.A., Shih, C.F., 1994. Plastic spin and related issues in phenomenological plasticity. ASME J. Appl. Mech. 61, 524–529.
Makinouchi, A., Nakamachi, E., Onate, E., Wagoner, R.H. (Eds.), 1993. NUMISHEET'93 Numerical Simulation of 3-D Sheet Metal Forming Processes—Verification of Simulation with Experiment. Proceedings of the 2nd International Conference, Isehara, Japan.
Oldroyd, J.G., 1950. On the formulation of rheological equations of state. Proc. Roy. Soc. Lond. A 200, 523.
Simo, J.C., 1988. A framework for finite strain elastoplasticity based on maximum plastic dissipation and the multiplicative decomposition: Part I. Continuum formulations. Comp. Meth. Appl. Mech. Eng. 66, 199–219.
Simo, J.C., Hughes, T.J.R., 1998. Computational Inelasticity. Springer.
Steinmann, P., Miehe, C., Stein, E., 1996. Fast transient dynamic plane stress analysis of orthotropic Hill-type solids at finite elastoplastic strains. Int. J. Solid Struct. 33, 1543–1562.
Truong Qui, K.H., Lippmann, H., 2000. Plastic spin and evolution of an anisotropic yield condition. Key Eng. Mat. 177–180, 13–22.
Truong Qui, K.H., Lippmann, H., 2001. On the impact of local rotation on the evolution of an anisotropic plastic yield condition. J. Mech. Phys. Sol. 49 (11), 2577–2591.
Tugcu, P., Neale, K.W., 1999. On the implementation of anisotropic yield functions into finite strain problems of sheet metal forming. Int. J. Plast. 15, 1021–1040.
Van der Giessen, E., 1991. Micromechanical and thermodynamical aspects of the plastic spin. Int. J. Plast. 7, 365–386.
Wagner, W., Gruttmann, F., 1994. A simple finite rotation formulation for composite shell elements. Eng. Comp. 11, 145–176.
Yang, D.Y., Kim, Y.J., 1986. A rigid-plastic finite element formulation for the analysis of general deformation of planar anisotropic sheet metals and its applications. Int. J. Mech. Sci. 12, 825–840.
Yoon, J.W., Yang, D.Y., Chung, K., 1999. Elasto-plastic finite element method based on incremental deformation theory and continuum based shell elements for planar anisotropic sheet materials. Comp. Meth. Appl. Mech. Eng. 174, 23–56.
Zbib, H.M., Aifantis, E.C., 1988. On the concept of relative and plastic spins and its implications to large deformation theories. Part I: hypoelasticity and vertex-type plasticity. Acta Mechanica 75, 15.